

An Antifatigue Liquid Metal Composite Electrode Ionic Polymer–Metal Composite Artificial Muscle with Excellent Electromechanical Properties

Zhihao He, Shasha Jiao, Zhengping Wang, Yifan Wang, Mengyu Yang, Ye Zhang, Yiwei Liu, Yuanzhao Wu, Jie Shang,* Qingming Chen,* and Run-Wei Li*



Cite This: <https://doi.org/10.1021/acsami.2c01453>



Read Online

ACCESS |



Metrics & More



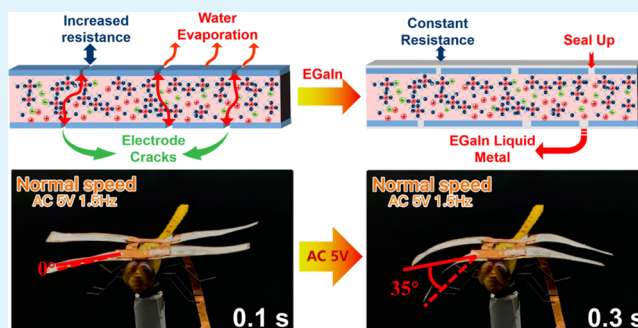
Article Recommendations



Supporting Information

ABSTRACT: Ionic polymer–metal composites (IPMC), one of the most popular materials in the field of artificial muscle research, have attracted much attention because of their high flexibility, low drive voltage (<10 V), high force density, large deformation, and so forth. However, the results show that the serious electrode fatigue crack and water loss of traditional IPMC greatly decrease its fatigue life and limit the practical application. In this study, we developed a novel liquid metal composite electrode. A layer of eutectic gallium–indium alloy (EGaIn) liquid metal was applied to the surface of the platinum electrode of the IPMC using a mask. Because of the good self-healing performance of the liquid metal, it is expected to solve the above problems of resistance increase and water loss caused by cracks. It turns out that the prepared EGaIn/Pt-IPMC exhibits a driving force up to 120 mN and maximum fatigue life of about 25,000 s at a driving voltage of 3 V. Compared with the best work reported, the fatigue strength of EGaIn/Pt-IPMC was increased by about 210%, and the maximum driving force of EGaIn/Pt-IPMC prepared by a single-layer basement membrane was between the IPMC prepared by 4–6 layer basement membrane. The electromechanical properties were significantly improved, and it is expected to realize a series of bionic applications.

KEYWORDS: liquid metal, eutectic gallium–indium, antifatigue, ionic polymer metal composites, driving force, tip displacement



1. INTRODUCTION

Since the 1990s, a new type of functional material, bionic artificial muscle material, has been rapidly developed and popularized both in academia and industry.^{1,2} This kind of material is designed with the concept of achieving biomimetic properties in nature by mimicking reversible deformation responses of living organisms under external conditions (voltage, current, temperature, pressure, light, humidity, and so forth), such as precise bending, twisting, and folding.^{3–13} Ionic polymerized metal composites (IPMC) are considered as the most promising artificial muscle for practical applications because of the low energy consumption, quick response, and large-angle bending under ultralow voltage (<10 V).^{14–19} Up to now, researchers at home and abroad have developed numerous soft-bodied robots with the similar biological ability of bionic functional characteristics based on IPMC. For example, Cohen et al. prepared the gold electrode IPMC with stronger electroactivity and invented a glass dust removal device according to the cyclic bending characteristics of IPMC under AC voltage.²⁰ Yu et al. used IPMC doped with carbon nanotubes to prepare a bionic gecko actuation system that enables internal and external toe flipping.²¹ Chen et al. cut and

spliced the polydimethylsiloxane film into the shape of manta rays and then attached platinum electrode IPMC on both sides of manta rays to realize free swimming under low power consumption.²²

IPMC has a typical sandwich structure composed of an ionized proton exchange membrane and metal electrodes on both sides.^{23,24} At present, the theory of hydration cation motion to explain the driving mechanism of IPMC has been generally recognized.^{21,23} According to the theory, the hydration cation in the membrane moves to the cathode side under the applied electric field, resulting in the aggregation and expansion of water molecules at the cathode side, the shrinkage of water shortage at the anode side, and the bending of IPMC to the anode side.^{25–27} However, when the IPMC was bent repeatedly countless times or the single-sided bending exceeds

Received: January 24, 2022

Accepted: March 7, 2022

the yield strain limit of the metal electrode, irregular fatigue cracks will occur randomly on the electrode surface (as shown in Figure 1a). The existence of these cracks will inevitably

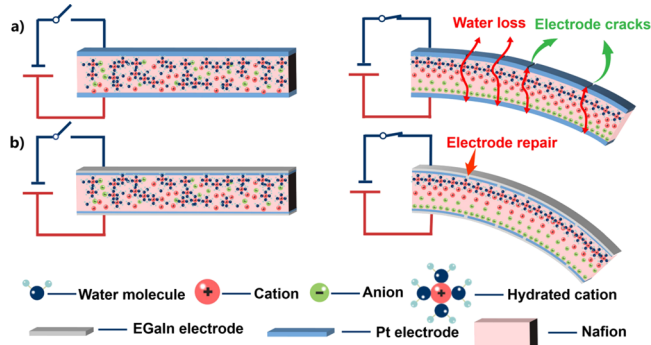


Figure 1. (a) Schematic diagram of IPMC-hydrated cation-driven bending theory. Conventional Pt-IPMC bends multiple times to produce electrode cracks, resulting in defects such as water loss in the film and increased electrode resistance. (b) EGaIn liquid metal was coated on the surface of Pt-IPMC to effectively fill the electrode cracks, as well as reduce the loss of water molecules in the film and surface electrode resistance.

increase the resistance of the electrode and produce an uneven electric field distribution, which significantly reduces the stable working time of IPMC and becomes the main factor affecting its practical applications.^{5,15,28–31} Therefore, researchers have also performed a lot of work to improve the fatigue life of IPMC. For example, Yu et al. achieved a fatigue life of up to 8200 s by coating the electrode with parylene and replacing the water solvent in the membrane with propylene carbonate as the solvent, thereby reducing the evaporation rate of the solvent in the membrane.³² Guo et al. coated conductive PEDOT on the electrode surface by electrochemical grafting, which, on the one hand, reduced the solvent evaporation rate in the film and, on the other hand, effectively filled the cracked electrode, reduced the electrode resistance change rate, and improved the performance stability of IPMC.³³ However, compared with the conductivity of traditional Pt, Au, or Cu electrodes ($\sim 10^8$ S m^{-1}), the electrode resistance after PEDOT repair is still much larger than that of the newly prepared electrode. In addition, the increase in the electrode

thickness with polymer coating also brings about a greater bending modulus, which will reduce the force-electric coupling performance of IPMC.^{24,34,35} Therefore, it is an urgent need to find a promising candidate with constant electrode resistance during the actuation process for the electrode material, which will not compromise the maximum bending displacement of the sample.

Here, a liquid metal electrode material called eutectic gallium–indium alloy (EGaIn) was reported, which has a wide liquid temperature range (15.9–2400 °C), high conductivity (3.46×10^6 S m^{-1}), and large surface tension (670 mN m^{-1}).^{36–38} The gallium-based liquid metal was deposited on the surface of the platinum electrode of the IPMC by using a mask version (as shown in Figure 1b). It was not only possible to prevent electrode cracking but also to improve the fatigue life of the IPMC. It was also worth noting that IPMC with gallium-based liquid metal electrodes have even better and more stable force-electric coupling properties compared to their counterparts, including a larger unilateral tip displacement (up to 41.04 mm), larger driving force (120 mN), and longer stable working time (25,000 s). Because of the superior performances of liquid metal-electrode-IPMC, a series of bionic functional demonstrations was expected to come true in more scenarios and make IPMC artificial muscles have greater possibilities in practical applications of software robots and future biomedicine.

2. RESULTS AND DISCUSSION

In this study, Ga-based liquid metal was chosen as the experimental material of the IPMC electrode. Here, metallic gallium and indium were introduced to prepare EGaIn alloy with a lower melting point.³⁶ Compared with traditional IPMC solid electrode materials, liquid metal has good fluidity, so the electrode coated with liquid metal has good self-healing performance.³⁹ Solid-state electrodes such as copper and platinum prepared by electrochemical reduction were composed of many nanometal particles strongly combined, which can provide a large specific surface area.⁴⁰ Therefore, eutectic gallium indium alloy and platinum (EGaIn/Pt) composite electrodes were used in this study, which could not only guarantee the stable resistance value in the actuation process⁴¹ but also bring greater specific capacitance value by the virtue of the nanoparticle structure of the platinum

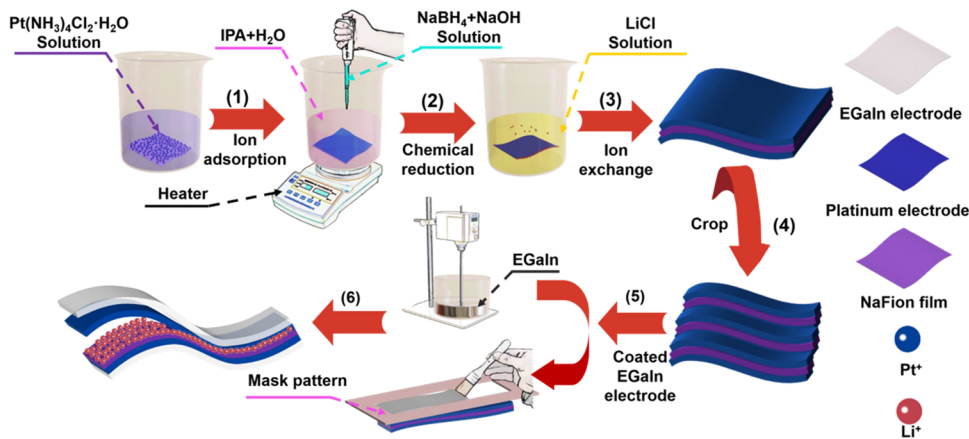


Figure 2. Preparation flow chart of EGaIn/Pt-IPMC, including (1) soaking in platinum ammonium ions for 24 h. (2) Alcohol-assisted chemical reduction of the Pt electrode. (3) Soaking for 24 h for the Li^+ -ion exchange process. (4) Cutting into 10 mm \times 50 mm strips. (5) EGaIn electrode was prepared and coated on the sample surface. (6) Obtaining the EGaIn/Pt-IPMC artificial muscle driver.

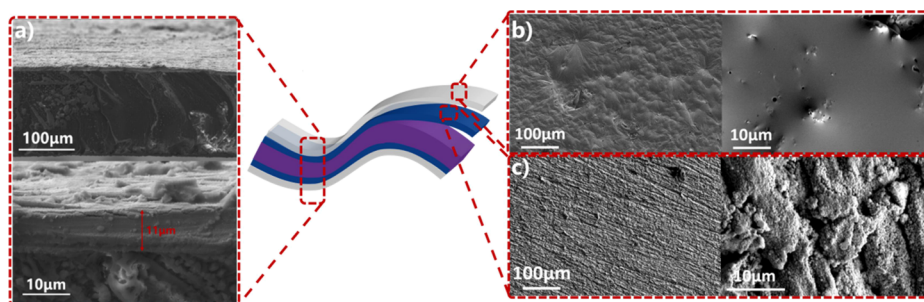


Figure 3. (a) EGaln/Pt-IPMC cross-section morphology. (b) EGaln electrode under a scanning electron microscope, and the surface morphology was smooth and flat, with no holes. (c) Platinum electrode under a scanning electron microscope, and the surface was composed of highly dense nanoparticles of the platinum electrode.

electrode so that IPMC actuators could have a faster response time, a longer stable operation time, and promote the migration efficiency of hydrated cations in the membrane.^{42–45}

In this work, DuPont Nafion membrane was used as the basement membrane. The basement membrane was pretreated before preparation. First, the surface of the Nafion membrane is roughened. Then, impurities are removed by ultrasonic and chemical methods. Finally, it is put into the solution for ion adsorption (as shown in Figure 2, the detailed parameters and steps are given in the Experimental section), and Pt-IPMC was fabricated by isopropanol-assisted chemical reduction plating to obtain strongly dispersed Pt electrodes.^{46,47} Because of the high conductivity of the liquid metal in the composite electrode, only an alcohol-assisted reduction of a thin platinum electrode layer was required, and then, EGaln/Pt-IPMC was obtained using the mask coating method. As can be seen in Figure 3a, EGaln/Pt-IPMC has a typical sandwich structure, with the total thickness of the EGaln/Pt composite electrode being only 11 μm . In addition, from the scanning electron microscopy (SEM) image of the electrode surface morphology, it can be seen that the surface of the top EGaln liquid metal electrode (Figure 3b) was smooth and free of small holes, which is more conducive to reducing the evaporation of water molecules from the film. Also, it was obvious (Figure 3c) that the intermediate electrode layer was a platinum particle film of nanosize, which makes it have a larger specific surface area of the electrode.

2.1. Electromechanical Property Test. The electromechanical properties were an important performance parameter of IPMC, including the tip displacement (the tip displacement was defined in Figure 4a), driving force, and other parameters. To accurately measure the tip displacement of IPMC, a laser displacement measurement system (Figure S1, Supporting Information) was established, which was composed of a laser displacement sensor, a signal generator, displacement acquisition, and recording software. Before the test, the IPMC was treated in 1 mol L⁻¹ LiCl solution for ion exchange for 24 h. The relationship curve between the tip displacement and time was tested in the form of a square wave at the frequency of 0.1–1 Hz under an AC voltage of 3 V (as shown in Figure 4b). It was clear that the peak-to-peak value of the displacement curve of EGaln/Pt-IPMC was about 32 mm with a frequency of 0.1 Hz, and it shows the typical symmetric drive of IPMC.³³

In addition, the tip displacement of EGaln/Pt-IPMC was measured at 1–5 V AC voltage in the form of a square wave with a frequency of 0.1 Hz (as shown in Figure 4c). The results show that the tip displacement of EGaln/Pt-IPMC increases

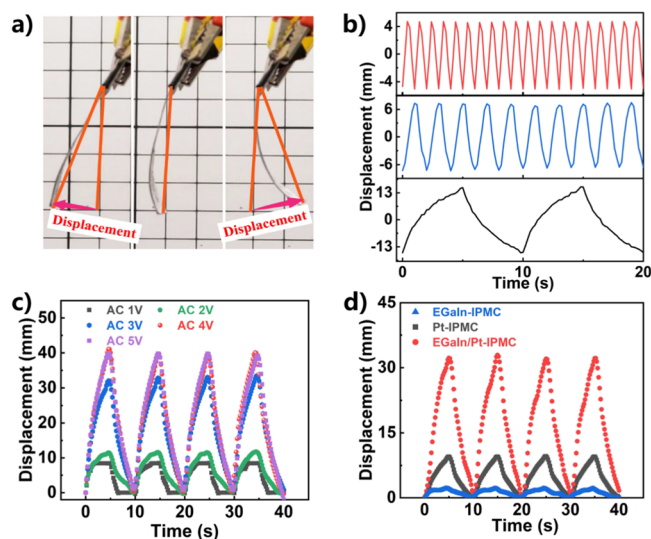


Figure 4. (a) Definition of tip displacement. (b) Relationship curve between the tip displacement and time was tested in the form of the square wave at the frequency of 0.1–1 Hz at the AC voltage of 3 V. (c) Tip displacement of EGaln/Pt-IPMC was measured at 1–5 V AC voltage in the form of a square wave with a frequency of 0.1 Hz. (d) Tip displacements of EGaln-IPMC, Pt-IPMC, and EGaln/Pt-IPMC at an AC voltage of 3 V, frequency 0.1 Hz.

with the increase in the applied voltage within a certain range and reaches the maximum displacement range value of 40 mm at an AC voltage of 4 V. When the voltage continues increasing up to 5 V, the tip displacement of EGaln/Pt-IPMC no longer increases. It is the reason that all hydrate cations in the membrane have migrated to the unilateral electrode area with the increase in the voltage amplitude.^{17,26} Furthermore, for comparison, Figure 4d shows the variation of the tip displacement along with the time of the IPMC driver based on different electrodes. It can be seen that EGaln/Pt-IPMC exhibited the best driving performance with the maximum driving displacement range of 32 mm at an AC voltage of 3 V and a frequency of 0.1 Hz.

On the other hand, an IPMC driving force test system was established and used a highly sensitive Instron pressure probe to accurately measure the IPMC driving force, which is displayed in Figure 5a. We first tested the driving force of EGaln/Pt-IPMC at different driving voltage amplitudes. From Figure 5b,d, it can be seen that the driving force of EGaln/Pt-IPMC increases with the increase in the driving voltage, and its maximum driving force is about 180 mN at a DC voltage of 5 V. However, it can be found that the decay speed of the driving

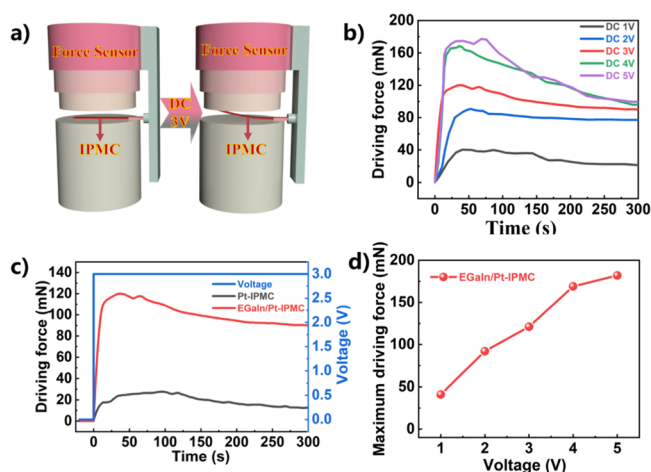


Figure 5. (a) IPMC driving force test system. (b) Driving force of EGAIn/Pt-IPMC as a function of time under the driving voltage of DC 1–5 V. (c) Driving force of EGAIn/Pt-IPMC and Pt-IPMC as a function of time at the DC voltage of 3 V. (d) Maximum driving force curves of EGAIn/Pt-IPMC at different driving voltages.

force was also proportional to the driving voltage. We consider that the increase in the driving voltage accelerates the electrolysis rate of water molecules in the membrane. In addition, it can be seen from Figure 5c that EGAIn/Pt-IPMC based on the composite electrode has a greater driving force (~ 120 mN), which is 300% higher than that of single-electrode Pt-IPMC. In addition, we also compared it with the best performance at present. The maximum driving force of EGAIn/Pt-IPMC prepared by the single-layer basement membrane was between the IPMC prepared by 4–6 layer basement membranes in a comparison work (as shown in Table 1).⁴⁸ Because the 3 V driving voltage is often used as the

Table 1. Driving Force of EGAIn/Pt-IPMC (190 μm) Was Compared with the Reported Work at Present (the Basement Membrane Thickness of the Comparison Work Was 780 and 1160 μm , Respectively)

	voltage (V)	driving force (mN)
Pt-IPMC (1160 μm)	4	190
Pt-IPMC (780 μm)	4	80
EGAIn/Pt-IPMC (190 μm) (this work)	3	120

experimental parameter condition in the existing research, in order to better compare with the existing research, the subsequent experiments all use the 3 V driving voltage as the test condition.

The bending displacement and driving force of IPMC are affected by many factors, including but not limited to electrode conductivity, IPMC-specific capacitance, moisture content of the basement membrane, and so forth.⁴⁹ When a layer of EGAIn liquid metal is used alone as the electrode of IPMC, the EGAIn liquid metal cannot provide a huge specific surface area like the nanoparticle platinum electrode of Pt-IPMC. Therefore, there was a big difference in the specific capacitance values of EGAIn-IPMC and Pt-IPMC (as shown in Figure 7b,c), and the resistivity difference between the EGAIn-IPMC and Pt-IPMC was relatively small; this is the reason why the EGAIn-IPMC shows the lower bending displacement and driving force.

2.2. Antifatigue Performance Test. Whether IPMC can work stably for a long time is a core practical problem for IPMC actuators.^{25,33} In this study, the displacement changes in EGAIn/Pt-IPMC, Pt-IPMC, and EGAIn-IPMC were measured using a laser displacement measurement system. To facilitate the analysis, the displacement data were normalized uniformly, and the fact that the time-normalized displacement attenuates to 0.1 was defined as the fatigue lifetime.^{32,33} Figure 6a shows

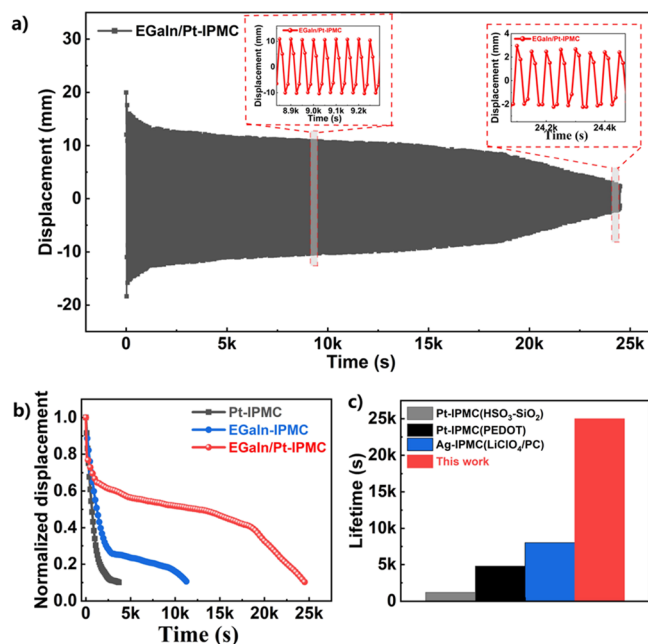


Figure 6. (a) Tip displacement curves of EGAIn/Pt-IPMC samples driven at an AC voltage of 3 V, frequency 0.02 Hz with time. (b) Normalized displacement curves of EGAIn/Pt-IPMC, Pt-IPMC, and EGAIn-IPMC with time driven at an AC voltage of 3 V, frequency 0.02 Hz. (c) Lifetime of EGAIn/Pt-IPMC compared to the existing work.

that the tip displacement curve varied with the time of the EGAIn/Pt-IPMC sample driven by AC voltage. It can be seen that the maximum tip displacement range can reach -20 to 20 mm, and EGAIn/Pt-IPMC can still maintain a driving distance of -3 to 3 mm after 24,500 s, showing good fatigue resistance. Compared to the control experimental group (Figure 6b), EGAIn-IPMC could not provide a large specific capacitance because of its low specific surface area,⁵⁰ making the fatigue life of EGAIn-IPMC only about 12000 s. On the contrary, the electrode of Pt-IPMC was composed of a layer of strongly connected platinum nanoparticles, which can provide a large specific surface area and mass-specific capacitance and promote the directional migration of hydrate cations. However, the large initial resistance and the increasing bending cracks of the Pt nanoparticle electrode lead to the number of directionally migrated hydrated cations in the membrane decreasing under the action of the electric field, which is the reason for the significant decrease in the bending stress and the displacement range of Pt-IPMC. EGAIn/Pt-IPMC mainly shows two significant properties: high specific capacitance and low initial resistivity. Because of the wide liquid temperature region of liquid metal, the electrodes of IPMC show good self-healing performance and stable resistance performance under bending strain. Therefore, EGAIn/Pt-IPMC can achieve a maximum fatigue time of 25,000 s, as shown in Figure 6c. Compared with

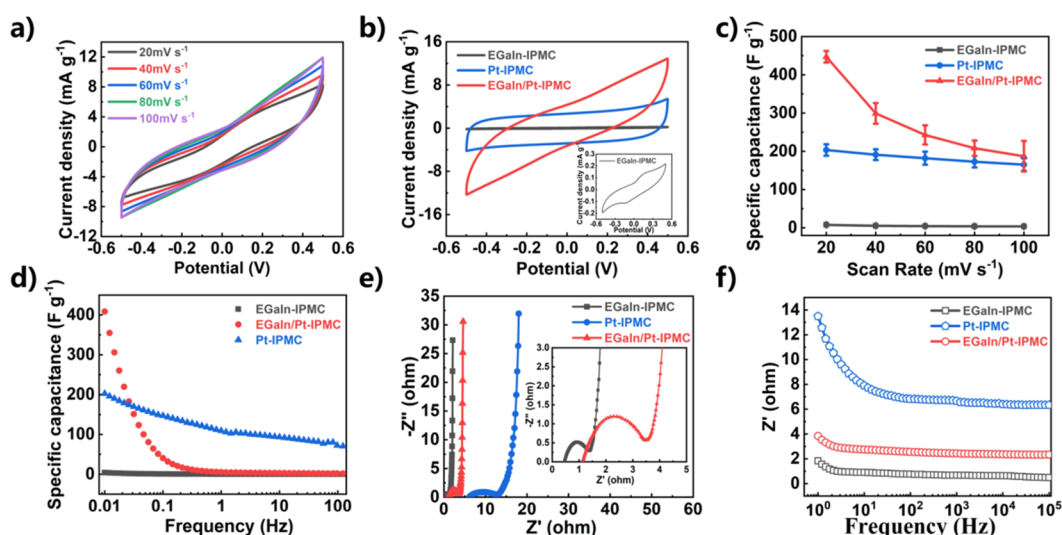


Figure 7. (a) CV curves of EGaIn/Pt-IPMC at the scanning speed of 20–100 mV s^{-1} . (b) CV curves of the three samples at the scanning speed of 100 mV s^{-1} . (c) Specific capacitance at the scanning speed of 20–100 mV s^{-1} . (d) Specific capacitance value of the EIS test. (e) Nyquist plots of the three samples. (f) Bode plots of the three samples.

the report of Han et al., doped nano- SiO_2 particles into perfluorosulfonic film (1200 s) has increased by 1600%; in Guo et al.'s work of PEDOT-coated electrodes (4800 s), it increased by 400%, and in the work of Yu et al. (8200 s) of replacing the water solvent in the membrane with propylene carbonate (PC), it increased by 210%.^{32–34}

Based on the excellent performances of liquid metal, research on IPMC restoration work has also been conducted. Aiming at the fatigue cracks of the traditional Pt-IPMC electrode caused by the excessive bending strain or excessive bending times, the samples cannot meet the status quo of sequential use. To address this, the surface of Pt-IPMC was coated with EGaIn liquid metal to repair the cracked platinum electrode (Figure S2a and S2b, Supporting Information). Then, the resistance of the Pt-IPMC (Cracked) electrode decreased from the maximum of 50 Ω to about 0.1 Ω (Figure S3a, Supporting Information), demonstrating the excellent electrical conductivity. In addition, the unrepaired cracked Pt-IPMC takes nearly 100 s to achieve the maximum driving force of 15 mN, while the Pt-IPMC (Cracked) only takes about 25 s to achieve the maximum driving force of 35 mN (Figure S3b, Supporting Information). The driving force of Pt-IPMC (Cracked) coated with EGaIn liquid metal was 133% higher than that without being coated. Moreover, the fatigue life of the cracked Pt-IPMC before and after coating EGaIn liquid metal is shown in Figures S4a and S4b (Supporting Information). It was not difficult to find that the Pt-IPMC (Cracked) repaired by EGaIn liquid metal can work stably for more than 20,000 s in the air, which is 700% longer than the service life of 2500 s before repair. It fully shows the great potential of EGaIn liquid metal in improving the antifatigue performance of IPMC.

2.3. Electrochemical Performance Test. Through physical model analysis, IPMC with a sandwich structure can be equivalent to a double-layer capacitor.^{42,51} Mass-specific capacitance is one of the key indexes to characterize the performances of the capacitor.^{52,53} The electrochemical properties of EGaIn/Pt-IPMC were tested using an electrochemical workstation, including EGaIn-IPMC and Pt-IPMC. Figure 7a shows the typical reversible cyclic voltammetry (CV)

curves of the double-layer capacitor. It was not difficult to find that in the applied voltage range of -0.5 to 0.5 V, EGaIn/Pt-IPMC exhibits quasi-ideal electric double-layer capacitance behavior at scanning speeds of 20–100 mV s^{-1} .^{39,54} Moreover, at the scanning speed of 100 mV s^{-1} , the CV Curve of three types of IPMC shows that EGaIn-IPMC has the largest rectangular area (Figure 7b). Especially when the scanning speed was 20 mV s^{-1} , the extremely large specific surface area of the EGaIn/Pt-IPMC electrode makes it exhibit a large weight-to-weight capacitance of 450 F g^{-1} (Figure 7c). Excellent capacitance performance can effectively promote the diffusion of electrolyte ions in the membrane and provide superior bending performances. According to the electrochemical impedance spectroscopy (EIS) test, the maximum specific capacitance was 403 F g^{-1} at a low frequency (Figure 7d), which is equivalent to the value calculated by the CV curve. In addition, as shown in the Nyquist plots shown in Figure 7e, the intercept of the curve on the X-axis represents the electrode resistance of IPMC.⁵⁵ It can be seen from the figure that the resistance of EGaIn liquid metal is about 0.1 Ω , and the nanoparticle platinum electrodes prepared using a dipping-reduction method generally around 5–20 Ω .⁵⁶ Meanwhile, the EGaIn Liquid metal can effectively fill the electrode pores and cracks, increase the conductive path, and reduce the resistance of the Pt electrode. Therefore, the actual resistance trend from high to low is Pt-IPMC, EGaIn/Pt-IPMC, and EGaIn-IPMC. Figure 7e shows the Nyquist plots for three types of IPMCs. In this case, EGaIn/Pt-IPMC exhibits a typical double-layer capacitance characteristic curve, which, in combination with Figure 7f, shows that EGaIn/Pt-IPMC exhibits an impedance down to about 4 Ω at 1/4 circle at low frequencies.⁴⁶

2.4. Electrode Resistance and Flexural Modulus Test. Combined with the analysis of the electrochemical performance test results of IPMC, it was known that the high specific capacitance and low impedance parameters have a positive effect on the performance of IPMC. However, as an academically accepted hyperelastic material,^{57,58} its nonlinear deformability was also influenced by a variety of external factors.⁵⁸ Therefore, to explore the various influencing factors

for high response deformation, high driving force, and fatigue resistance, the surface electrode resistance, film water content, and bending modulus of EGaIn/Pt-IPMC were tested in relation to each other. The experimental protocol and results of the electrode resistance tests are shown in Figure 8a,b. The

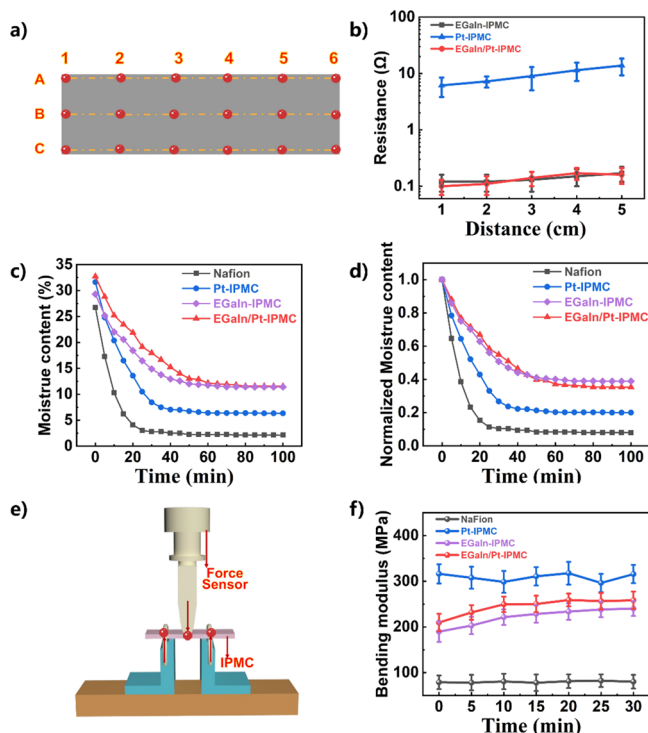


Figure 8. (a) Schematic diagram of the IPMC surface resistance scheme test, (b) surface resistance variation curves for EGaIn-IPMC, Pt-IPMC, and EGaIn/Pt-IPMC. (c) Moisture content test for Nafion film, Pt-IPMC, EGaIn-IPMC, and EGaIn/Pt-IPMC. (d) Normalized moisture content curves for IPMC over time. (e) Bending modulus of IPMC measured using the three-point bending method. (f) Bending modulus curve for Nafion substrate film, EGaIn-IPMC, Pt-IPMC, and EGaIn/Pt-IPMC over time.

electrode resistance of EGaIn/Pt-IPMC was quite low ($\sim 0.1 \Omega$), which is much lower than the conventional Pt-IPMC electrode resistance ($\sim 10 \Omega$). The Pt electrode of IPMC is obtained using the impregnation–reduction method, and a thin film electrode was formed by closely stacking numerous nano-Pt particles, so its resistance value cannot be as low as that of the Pt electrode prepared using the traditional melting method. Combined with the literature and a large number of test results, the resistance of platinum electrodes prepared using the dipping–reduction method generally fluctuates around $5\sim 20 \Omega$,^{28,33,56} but the resistance of EGaIn liquid metal electrodes can be as low as $\sim 0.1 \Omega$. Therefore, as shown in Figure 8b, the surface resistance of the Pt-IPMC is significantly higher than that of the EGaIn-IPMC. The relationship between resistivity and charge is shown in formula 1:

$$\frac{dQ}{dt} = \frac{VLB}{2h\rho} \quad (1)$$

In formula 1, Q is the electrode charge, V is the driving voltage applied to the electrode, L is the length of the electrode, B is the width of the electrode, h is the thickness of the electrode, and ρ is the resistivity of the electrode.

It can be seen that lower resistivity helps increase the number of freely movable charges per unit time in the electrode, thereby promoting the directional migration of more hydrated cations in the basement membrane and improving the response speed and bending strength of IPMC. This also means that under the same driving voltage, much more freely moving electrons can be activated on the EGaIn/Pt-IPMC electrode, and more water and cations in the film can be adsorbed to gather on the cathode side of the IPMC, thereby generating a larger angle of bending deformation.

Therefore, according to the theory of hydrated cation migration, the content of water molecules in the membrane plays a crucial role in the bending of IPMC. The water contents of Pt-IPMC, EGaIn-IPMC, and EGaIn/Pt-IPMC were tested using the weighing method with the following equations:

$$W = \frac{M_{\text{wet}} - M_{\text{dry}}}{M_{\text{dry}}} \times 100\% \quad (2)$$

In formula 2, M_{wet} is the weight of IPMC that fully absorbs moisture, M_{dry} is the weight of IPMC after drying, and W is the moisture content.

Through experiments, the moisture content change curve of IPMC has been established, as shown in Figure 8c,d. Based on the wide liquid-phase temperature range of liquid metal, EGaIn-IPMC, and EGaIn/Pt-IPMC can effectively prevent the evaporation of water molecules from the film. Especially for platinum electrodes made of platinum nanoparticles, there were a lot of pores on their surface, and the presence of liquid metal can effectively fill the pores, reduce the evaporation path of water molecules, and ensure the number of water molecules directionally migrating in the membrane.

On the other hand, because of the different materials used for IPMC electrodes, their flexural modulus varies. An excessively high flexural modulus will severely limit the drive performance of IPMC and affect the practical application of IPMC. Therefore, the Instron universal testing machine was used to test the flexural modulus of IPMC (as shown in Figure 8e), where the flexural modulus formula of IPMC can be expressed as follows:

$$C3P = \frac{L^3}{48*I} * s \quad (3)$$

$$I = \frac{a*h^3}{12} \quad (4)$$

$$s = \frac{F}{\Delta L} \quad (5)$$

where $C3P$ is the elastic modulus value measured using the three-point bending method,⁵⁹ a is the width of the IPMC, h is the thickness, s is the elastic ratio, L is the two-point span, F is the force measured by the testing machine value, and ΔL is the amount of displacement change.

In the experiments, three control experimental groups were set up, namely, Nafion substrate film, Pt-IPMC, and EGaIn-IPMC. According to the analysis of the experimental data (Figure 8f), the bending modulus of the composite electrode EGaIn/Pt-IPMC prepared by primary chemical plating was about 250 MPa, which is smaller than that of the conventional secondary chemical plating of Pt-IPMC (~ 325 MPa).

Therefore, the lower bending stress of EGaIn/Pt-IPMC allows for greater bending deformation.

2.5. IPMC Bionic Applications. In this research, EGaIn/Pt-IPMC has an excellent performance in terms of fatigue life, driving displacement, and driving force. In turn, a series of demonstration applications based on the IPMC actuation performance was designed and prepared. First, a bionic fishtail has been designed that can oscillate from side to side at an AC voltage of 5 V and a frequency of 1.5 Hz. (video clip S1, Supporting Information). The maximum oscillation amplitude can reach around ± 10 mm (Figure 9a), thus promising a

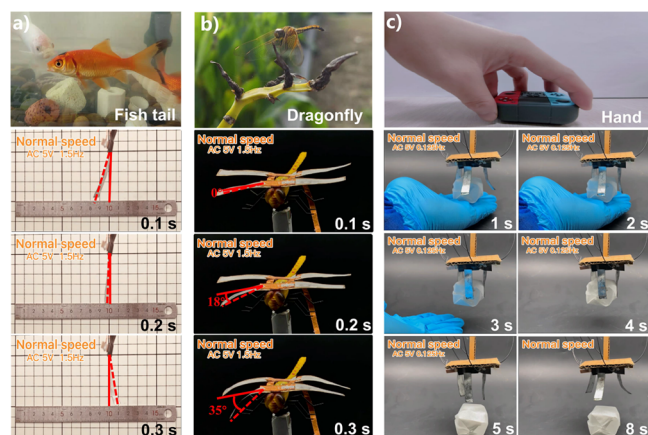


Figure 9. (a) Driving effect of bionic fishtail at an AC voltage of 5 V, frequency of 1.5 Hz. (b) Driving demonstration of bionic dragonfly at an AC voltage of 5 V, frequency of 1.5 Hz. (c) Effect demonstration of bionic artificial hand-grasping paper lantern at an AC voltage of 5 V, frequency 0.125 Hz.

motorless high-frequency, large-amplitude bionic drive. Second, a dragonfly-like soft robot was prepared based on the high-frequency and large-amplitude driving characteristics of EGaIn/Pt-IPMC (Figure 9b). The constructed bionic dragonfly wings exhibit stable wing-flapping motion at an AC voltage of 5 V and a frequency of 1.5 Hz. (video clip S2, Supporting Information), and the maximum wingspan angle can reach 35° . Finally, a bionic artificial hand was designed and fabricated to mimic human grasping behavior, as shown in Figure 9c (video clip S3, Supporting Information). When a forward voltage is applied, the bionic artificial hand transforms from a free vertical state to a flexible “outward expansion” state. When changing the current direction, the bionic artificial hand change from the “extended” state to the “clamping” state. The entire process of grabbing paper lanterns can be completed in 8 s without any mechanical structure. It has the characteristics of low energy consumption, light weightness, and no noise. The demonstration application of EGaIn/Pt-IPMC shows that it has great potential for commercial applications in the fields of underwater soft robots, micro-aircraft, and industrial flexible grippers.

3. CONCLUSIONS

This study demonstrates an IPMC driver based on the EGaIn/Pt composite electrode, which enhances the bending strain, driving force, and fatigue life of IPMC through the synergistic effect of the Pt electrode and the gallium–indium liquid metal electrode. Because of the high conductivity and wide liquid-phase temperature of the EGaIn liquid metal electrode and the large specific surface area of the nano-Pt electrode, the

electrode surface resistance of EGaIn/Pt-IPMC always maintains a low rate of change, while exhibiting a large mass-specific capacitance value of up to 450 F g^{-1} , forming a quasi-ideal electric double-layer capacitance that effectively promotes ion migration in IPMC. The prepared EGaIn/Pt-IPMC artificial muscle actuator exhibited a driving force of up to 120 mN and a maximum driving displacement of 32 mm at a driving voltage of 3 V. In particular, the fatigue life value, which still exhibits a driving displacement of ± 3 mm at about 25,000 s, is 210% of that of the currently reported hydrated cation-migrating type of IPMC. In addition, EGaIn liquid metal can also perform the electrode repair for crack-generating IPMC to some extent, showing considerable economy. Finally, based on the excellent performance of EGaIn/Pt-IPMC in several aspects, three bionic applications were demonstrated, showing their great application potential and prospects in the field of soft robotics.

4. EXPERIMENTAL SECTION

4.1. Preparation of EGaIn/Pt-IPMC. The Nafion 117 membrane (from DuPont, USA) was pretreated, and both sides of the base membrane were polished with sandpaper (model: Eagle 1000 mesh, Hubei Chengli Abrasives Co., Ltd.). The sample was put into a numerically controlled ultrasonic cleaner (model KQ-500DE, Kunshan Ultrasonic Instrument Co., Ltd.) for ultrasonic cleaning, soaked in a 5 wt % HCl (30%, Sinopharm Chemical Reagent Co., Ltd.) aqueous solution for 1 h, taken out, soaked in 5 wt % H_2O_2 (30%, Shanghai Aladdin Biochemical Technology Co., Ltd.) aqueous solution for 1 h, finally soaked in distilled water at 80°C for 30 min, then taken out, added 0.5 wt % $\text{Pt}(\text{NH}_3)_4\text{Cl}_2$ (anhydrous, Shanghai Aladdin Biochemical Technology Co., Ltd.) soaked in an aqueous solution for 48 h, and shaded with tin foil. The treated Nafion 117 film was placed in a mixed solution of isopropanol ($\text{C}_3\text{H}_8\text{O}$, 99.8%, Shanghai Aladdin Biochemical Technology Co., Ltd.) and deionized water in a volume ratio of 1:3, and it was placed under magnetic heating and stirring. When the film was fully swelled by the swelling effect of alcohol on the device (model: C-MAG HS7, IKA company, Germany), it was heated to 40°C , and 2 mL of 5 wt % NaBH_4 (98%, Sinopharm Chemical Reagent Co., Ltd.) was added. For the aqueous solution, the magnetic stirring function was turned on, 2 mL of 5 wt % NaBH_4 aqueous solution was added every 30 min, and the heating temperature was increased by 3°C . When the temperature reached 62°C , 10 mL of 5 wt % NaBH_4 aqueous solution was added and heated at a constant temperature for 1 h. A dense and uniform nanodispersed Pt electrode layer was chemically reduced on the surface of the film. The prepared Pt-IPMC was placed in 5 wt % HCl for 10 h, placed in 80°C deionized water, and heated for 2 h to ensure that the ammonium ions in the membrane were removed. Finally, Pt-IPMC was put into 1 mol/L LiCl (99.0%, Shanghai Aladdin Biochemical Technology Co., Ltd.) aqueous solution, and sufficient ion exchange was conducted for 48 h. On the other hand, high-purity metallic gallium (99.99%, Yingtian Mailin Gallium Industry Co., Ltd.) and high-purity metallic indium (99.995%, Beijing Fangde Xingchen Technology Co., Ltd.) were mixed at a mixing ratio of 3:1. An electric stirrer (model: JB300-D, manufactured by Shanghai Specimen Model Factory) was used to stir and mix for 90 min at a speed of 100 rpm, and the well-mixed liquid metal of EGaIn was coated on both sides of the Pt electrode surface through a mask to obtain EGaIn/Pt-IPMC.

4.2. Electromechanical Property Test. In the electromechanical property test, the EGaIn/Pt-IPMC was cut into strips with a width of 10 mm and a length of 50 mm. The stress test system was composed of Keithley power supply (model: Keithley 237, Tektronix) to provide a DC voltage, a voltage range (-220 to 220 V), and an ultrasensitive stress probe (model: force detection range 0~500 N). The displacement test system was measured using a built-up laser displacement sensor system. The laser displacement sensor (model: HG-C1200, Matsushita Electric Industrial Co., Ltd.) and the signal generator (model: AFG3101C, Tektronix) provided AC power, and

the voltage frequency range (0.01 Hz~100 MHz), data acquisition controller (model: DAQ-280G, Shanghai Pinxu Industrial Co., Ltd.), and the matching Labview measurement data acquisition software were applied.

4.3. Characterization. SEM (model: Sirion200, FEI) was used to study and analyze the surface morphology and cross-section morphology of EGaIn/Pt-IPMC. The CV curve and EIS spectrum of IPMC were tested. The CV curve and EIS performance test analysis of IPMC spline was performed using the electrochemical workstation (CHI660E, Shanghai Chenhua Instrument Co., Ltd.) three-electrode method, the test voltage range of CV was -0.5 to 0.5 V, the scan speed was $20\sim 100$ mV S^{-1} , the mass m of different IPMC was measured, and the IPMC mass-specific capacitance value can be obtained according to formula 6:

$$C = \frac{\int_{V_1}^{V_2} i dV}{2mv(V_2 - V_1)} \quad (6)$$

In the above formula, i is the scan current in the CV curve, V_1 and V_2 are the initial voltage and the end voltage of the scan, m is the quality of the IPMC, and v is the voltage scan rate. The numerator part represents the area enclosed by the CV curve. In addition, the IPMC mass-specific capacitance was tested using an impedance analysis tester (model: IM3570, HIOKI), and the test frequency was in the frequency range of 0.1 to 100 Hz. The AC disturbance voltage amplitude of the instrument was set to 10 mV, and the DC bias voltage was set to 0.1 V, so the calculation formula of the differential electric double layer capacitance $C_d(f)$ of IPMC is shown in formula 7:

$$C_d(f) = \frac{-1}{2\pi m f Z''(f)} \quad (7)$$

In the above formula, m is the mass of the IPMC sample, f is the frequency of the AC voltage, and $Z''(f)$ is the measured imaginary part of the impedance.

■ ASSOCIATED CONTENT

SI Supporting Information

The Supporting Information is available free of charge at <https://pubs.acs.org/doi/10.1021/acsami.2c01453>.

Additional performance characterization data for EGaIn/Pt-IPMC, such as the effect of drive voltage frequency and amplitude on displacement, and the ability of EGaIn to repair cracked electrode IPMC (including drive force enhancement and fatigue displacement enhancement) (PDF)

Imitating fish tail wobble (MP4)

Imitating dragonfly wings (MP4)

Bionic artificial hand (MP4)

High-amplitude high-frequency swing (MP4)

■ AUTHOR INFORMATION

Corresponding Authors

Jie Shang – CAS Key Laboratory of Magnetic Materials and Devices and Zhejiang Province Key Laboratory of Magnetic Materials and Application Technology, Ningbo Institute of Materials Technology and Engineering Chinese Academy of Sciences, Ningbo 315201, P. R. China; orcid.org/0000-0003-0996-1038; Email: shangjie@nimte.ac.cn

Qingming Chen – Faculty of Materials Science and Engineering, Kunming University of Science and Technology, Kunming 650093, P. R. China; Email: 16855945@qq.com

Run-Wei Li – College of Materials Science and Opto-Electronic Technology, University of Chinese Academy of

Sciences, Beijing 100049, P. R. China; orcid.org/0000-0003-3879-9834; Email: runwei@nimte.ac.cn

Authors

Zhihao He – Faculty of Materials Science and Engineering, Kunming University of Science and Technology, Kunming 650093, P. R. China; CAS Key Laboratory of Magnetic Materials and Devices and Zhejiang Province Key Laboratory of Magnetic Materials and Application Technology, Ningbo Institute of Materials Technology and Engineering Chinese Academy of Sciences, Ningbo 315201, P. R. China

Shasha Jiao – CAS Key Laboratory of Magnetic Materials and Devices and Zhejiang Province Key Laboratory of Magnetic Materials and Application Technology, Ningbo Institute of Materials Technology and Engineering Chinese Academy of Sciences, Ningbo 315201, P. R. China

Zhengping Wang – CAS Key Laboratory of Magnetic Materials and Devices and Zhejiang Province Key Laboratory of Magnetic Materials and Application Technology, Ningbo Institute of Materials Technology and Engineering Chinese Academy of Sciences, Ningbo 315201, P. R. China

Yifan Wang – CAS Key Laboratory of Magnetic Materials and Devices and Zhejiang Province Key Laboratory of Magnetic Materials and Application Technology, Ningbo Institute of Materials Technology and Engineering Chinese Academy of Sciences, Ningbo 315201, P. R. China

Mengyu Yang – CAS Key Laboratory of Magnetic Materials and Devices and Zhejiang Province Key Laboratory of Magnetic Materials and Application Technology, Ningbo Institute of Materials Technology and Engineering Chinese Academy of Sciences, Ningbo 315201, P. R. China

Ye Zhang – CAS Key Laboratory of Magnetic Materials and Devices and Zhejiang Province Key Laboratory of Magnetic Materials and Application Technology, Ningbo Institute of Materials Technology and Engineering Chinese Academy of Sciences, Ningbo 315201, P. R. China

Yiwei Liu – CAS Key Laboratory of Magnetic Materials and Devices and Zhejiang Province Key Laboratory of Magnetic Materials and Application Technology, Ningbo Institute of Materials Technology and Engineering Chinese Academy of Sciences, Ningbo 315201, P. R. China; orcid.org/0000-0001-9355-5168

Yuanzhao Wu – CAS Key Laboratory of Magnetic Materials and Devices and Zhejiang Province Key Laboratory of Magnetic Materials and Application Technology, Ningbo Institute of Materials Technology and Engineering Chinese Academy of Sciences, Ningbo 315201, P. R. China

Complete contact information is available at:

<https://pubs.acs.org/doi/10.1021/acsami.2c01453>

Author Contributions

The manuscript was written through contributions of all authors. All authors have given approval to the final version of the manuscript.

Notes

The authors declare no competing financial interest.

■ ACKNOWLEDGMENTS

This research was partially supported by the National Natural Science Foundation of China (61774161, 51931011, 51971233, 62174165, M-0152, U20A6001, and U1909215), the External Cooperation Program of Chinese Academy of

Sciences (174433KYSB20200013, 174433KYSB20190038), the Instrument Developing Project of the Chinese Academy of Sciences (YJKYYQ20200030), K.C. Wong Education Foundation (GJTD-2020-11), Chinese Academy of Sciences Youth Innovation Promotion Association (2018334), CAS President's International Fellowship Initiative (PIFI) (2019PE0019), Zhejiang Provincial Key R&D Program (2021C01183), Public Welfare Technical Applied Research Project of Zhejiang Province (LGG19F010006), and Ningbo Scientific and Technological Innovation 2025 Major Project (2018B10057, 2019B10127, and 2020Z022).

REFERENCES

- (1) Wehner, M.; Truby, R. L.; Fitzgerald, D. J.; Mosadegh, B. G.; Whitesides, M.; Lewis, J. A.; Wood, R. J. An Integrated Design and Fabrication Strategy for Entirely Soft, Autonomous Robots. *Nature* **2016**, *536*, 451–455.
- (2) Shepherd, R. F.; Ilievski, F.; Choi, W.; Morin, S. A.; Stokes, A. A.; Mazzeo, A. D.; Chen, X.; Wang, M.; Whitesides, G. M. Multigait Soft Robot. *Proc. Natl. Acad. Sci. U. S. A.* **2011**, *108*, 20400–20403.
- (3) Mirvakili, S. M.; Hunter, I. W. Multidirectional Artificial Muscles from Nylon. *Adv. Mater.* **2017**, *29*, No. 1604734.
- (4) Gu, G. Y.; Zhao, J. R.; Zhao, X.; Zhu, X. Y. Soft Wall-Climbing Robots. *Sci. Robot.* **2018**, *3*, No. eaat2874.
- (5) Bhandari, B.; Lee, G. Y.; Ahn, S. H. A Review on IPMC Material as Actuators and Sensors: Fabrications, Characteristics and Applications. *Int. J. Precis. Eng. Manuf.* **2012**, *13*, 141–163.
- (6) Amjadi, M.; Sitti, M. Self-Sensing Paper Actuators Based on Graphite-Carbon Nanotube Hybrid Films. *Adv. Sci.* **2018**, *5*, No. 1800239.
- (7) Kizilkan, E.; Strueben, J.; Staubitz, A.; Gorb, S. N. Bioinspired Photocontrollable Microstructured Transport Device. *Sci. Robot.* **2017**, *2*, No. eaak9454.
- (8) Li, S. G.; Vgot, D. M.; Rus, D.; Wood, R. J. Fluid-Driven Origami-Inspired Artificial Muscles. *Proc. Natl. Acad. Sci. U. S. A.* **2017**, *114*, 13132–13137.
- (9) Mirvakili, S. M.; Pazukha, A.; Sikkema, W.; Sinclair, C. W.; Spinks, G. M.; Baughman, R. H.; Madden, J. D. W. Niobium Nanowire Yarns and Their Application as Artificial Muscles. *Adv. Funct. Mater.* **2013**, *23*, 4311–4316.
- (10) Zheng, J.; Xiao, P.; Le, X. X.; Lu, W.; Théato, P.; Ma, C. X.; Du, B. Y.; Zhang, J. W.; Huang, Y. J.; Chen, T. Mimosa Inspired Bilayer Hydrogel Actuator Functioning in Multi-Environments. *J. Mater. Chem. C* **2018**, *6*, 1320–1327.
- (11) Mirvakili, S. M.; Hunter, I. W. Fast Torsional Artificial Muscles from NiTi Twisted Yarns. *ACS Appl. Mater. Interfaces* **2017**, *9*, 16321–16326.
- (12) Zhao, Q.; Dunlop, J. W. C.; Qiu, X. L.; Huang, F. H.; Zhang, Z. B.; Heyda, J.; Dzubielka, J.; Antonietti, M.; Yuan, J. Y. An Instant Multi-Responsive Porous Polymer Actuator Driven by Solvent Molecule Sorption. *Nat. Commun.* **2014**, *5*, 4293–4301.
- (13) Amjadi, M.; Sitti, M. High-Performance Multiresponsive Paper Actuators. *ACS Nano* **2016**, *10*, 10202–10210.
- (14) Nemat-Nasser, S. Micromechanics of Actuation of Ionic Polymer-Metal Composites. *J. Appl. Phys.* **2002**, *92*, 2899–2915.
- (15) Shahinpoor, M.; Kim, K. J. Ionic Polymer-Metal Composites: I. Fundamentals. *Smart Mater. Struct.* **2001**, *10*, 819–833.
- (16) Nemat-Nasser, S.; Li, J. Y. Electromechanical Response of Ionic Polymer-Metal Composites. *J. Appl. Phys.* **2000**, *87*, 3321–3331.
- (17) Kim, K. J.; Shahinpoor, M. Ionic Polymer-Metal Composites: II. Manufacturing Techniques. *Smart Mater. Struct.* **2003**, *12*, 65–79.
- (18) Yu, M.; Shen, H.; Dai, Z. Manufacture and Performance of Ionic Polymer-Metal Composites. *J. Bionic Eng.* **2007**, *4*, 143–149.
- (19) Baughman, R. H. Playing Nature's Game with Artificial Muscles. *Science* **2005**, *308*, 63–65.
- (20) Bar-Cohen, Y.; Leary, S. P.; Yavrouian, A.; Oguro, K.; Tadokoro, S. S.; Harrison, J. S.; Smith, J. G.; Su, J. Challenges to the Application of IPMC as Actuators of Planetary Mechanisms. *Smart Mater. Struct.* **2000**, *3987*, 140–146.
- (21) Yu, M.; He, Q. S.; Yu, D. S.; Zhang, X. Q.; Ji, A. H.; Zhang, H.; Guo, C.; Dai, Z. D. Efficient Active Actuation to Imitate locomotion of Gecko's Toes using an Ionic Polymer-metal Composite Actuator Enhanced by Carbon Nanotubes. *Appl. Phys. Lett.* **2012**, *101*, 163701.
- (22) Chen, Z.; Um, T. I.; Bart-Smith, H. A Novel Fabrication of Ionic Poly-metal Composite Membrane Actuator Capable of 3-Dimensional Kinematic Motions. *Sens. Actuators, A* **2011**, *168*, 131–139.
- (23) Tiwari, R.; Garcia, E. The State of Understanding of Ionic Polymer Metal Composite Architecture: A Review. *Smart Mater. Struct.* **2011**, *20*, No. 083001.
- (24) Tiwari, R.; Kim, K. J. Effect of Metal Diffusion on Mechanoelectric Property of Ionic Polymer-Metal Composite. *Appl. Phys. Lett.* **2010**, *97*, 244104.
- (25) Wang, F.; Zhang, X. D.; Ma, L.; Zhang, Z. Q.; Han, L. F.; Zeng, C.; Shi, B.; Guo, D. J. Facile and Effective Repair of Pt/Nafion IPMC Actuator by Dip-coating of PVP@AgNPs. *Nanotechnology* **2021**, *32*, 385502.
- (26) Tadokoro, S. S.; Yamagami, S. J.; Takamori, T. S.; Oguro, K. S. Modeling of Nafion-Pt Composite Actuators (ICPF) by Ionic Motion. *Smart Mater. Struct.* **2000**, *3987*, 92–102.
- (27) Liu, Y.; Ghaffari, M.; Zhao, R.; Lin, J. H.; Lin, M.; Zhang, Q. M. Enhanced Electromechanical Response of Ionic Polymer Actuators by Improving Mechanical Coupling Between Ions and Polymer Matrix. *Macromolecules* **2012**, *45*, 5128–5133.
- (28) Guo, D. J.; Han, Y. B.; Huang, J. J.; Meng, E. C.; Ma, L.; Zhang, H.; Ding, Y. H. Hydrophilic Poly (Vinylidene Fluoride) Film with Enhanced Inner Channels for Both Water- and Ionic Liquid-Driven Ion-Exchange Polymer Metal Composite Actuators. *ACS Appl. Mater. Interfaces* **2019**, *11*, 2386–2397.
- (29) Guo, D. J.; Liu, R.; Cheng, Y.; Zhang, H.; Zhou, L. M.; Fang, S. M.; Elliott, W. H. Reverse Adhesion of a Gecko-inspired Synthetic Adhesive Switched by an Ion-Exchange Polymer-Metal Composite Actuator. *ACS Appl. Mater. Interfaces* **2015**, *7*, 5480–5487.
- (30) Guo, D. J.; Ding, H. T.; Wei, H. J.; He, Q. S.; Yu, M.; Dai, Z. D. Hybrids Perfluorosulfonic Acid Ionomer and Silicon Oxide Membrane for Application in Ion-Exchange Polymer-Metal Composite Actuators. *Sci. China, Ser. E: Technol. Sci.* **2009**, *52*, 3061–3070.
- (31) Tamagawa, H.; Watanabe, H.; Sasaki, M. Bending Direction Change of IPMC by the Electrode Modification. *Sens. Actuators, B* **2009**, *140*, 542–548.
- (32) Yu, C. Y.; Zhang, Y. W.; Su, G. D. J. Reliability Tests of Ionic Polymer Metallic Composites in Dry Air for Actuator Applications. *Sens. Actuator, A* **2015**, *232*, 183–189.
- (33) Guo, D. J.; Wang, L.; Wang, X. J.; Xiao, Y. N.; Wang, C. D.; Chen, L. M.; Ding, Y. H. PEDOT Coating Enhanced Electro-mechanical Performances and Prolonged Stable Working Time of IPMC Actuator. *Sens. Actuators, B* **2020**, *305*, No. 127488.
- (34) Han, Y. B.; Wang, F.; Li, H. K.; Meng, E. C.; Fang, S. M.; Zhao, A. S.; Guo, D. J. Sulfonic SiO₂ Nanocolloid Doped Perfluorosulfonic Acid Films with Enhanced Water Uptake and Inner Channel for IPMC Actuators. *RSC Adv.* **2019**, *9*, 42450–42458.
- (35) Akle, B. J.; Leo, D. J.; Hickner, M. A.; McGrath, J. E. Correlation of Capacitance and Actuation in Ionomeric Polymer Transducers. *J. Mater. Sci.* **2005**, *40*, 3715–3724.
- (36) Wang, X. L.; Guo, R.; Liu, J. Self-Powered Gallium-Based Liquid-Metal Beating Heart. *J. Phys. Chem. A* **2019**, *123*, 9268–9273.
- (37) Shu, J.; Ge, D.-A.; Wang, E. L.; Ren, H. T.; Cole, T.; Tang, S.-Y. A Liquid Metal Artificial Muscle. *Adv. Mater.* **2021**, *33*, No. 2103062.
- (38) Thrasher, C. J.; Farrell, Z. J.; Morris, N. J.; Willey, C. L.; Tabor, C. E. Mechanoresponsive Polymerized Liquid Metal Networks. *Adv. Mater.* **2019**, *31*, No. 1903864.
- (39) Chen, S.; Wang, H. Z.; Zhao, R. Q.; Rao, W.; Liu, J. Liquid Metal Composites. *Matter* **2020**, *2*, 1446–1480.
- (40) Li, R. B.; Yu, L. L.; Li, S.; Fan, J.; Luo, R.; Zhao, J. T. Facile Synthesis of Hierarchical Mesoporous Beta-Manganese Dioxide Nanoflowers With Extremely High Specific Surface Areas for High-

Performance Electrochemical Capacitors. *Electrochim. Acta* **2018**, *284*, 52–59.

(41) Tabor, C.; Holcomb, S.; Heikenfeld, J. Reliable and Reversible Contact of Eutectic Gallium Indium and Copper Electrodes. *Adv. Mater. Interfaces* **2020**, *7*, No. 1902182.

(42) Yang, L.; Zhang, D.; Wang, H.; Zhang, X. N. Actuation Modeling of Ionic-Polymer Metal Composite Actuators Using Micromechanics Approach. *Adv. Eng. Mater.* **2020**, *22*, No. 2000537.

(43) Yang, L.; Wang, H.; Zhang, X. N. Recent Progress in Preparation Process of Ionic Polymer-Metal Composites. *Results Phys.* **2021**, *29*, No. 104800.

(44) Kong, L.; Chen, W. Carbon Nanotube and Graphene-Based Bioinspired Electrochemical Actuators. *Adv. Mater.* **2014**, *26*, 1025–1043.

(45) Yang, L.; Zhang, D.; Zhang, X.; Tian, A. Electroless Copper Deposition and Interface Characteristics of Ionic Electroactive Polymer. *J. Mater. Res. Technol.* **2021**, *11*, 849–856.

(46) Ma, S. Q.; Zhang, Y. P.; Liang, Y. H.; Ren, L.; Tian, W. J.; Ren, L. Q. High-Performance Ionic-Polymer-Metal Composite: Toward Large-Deformation Fast-Response Artificial Muscles. *Adv. Funct. Mater.* **2020**, *30*, No. 1908508.

(47) Liu, H.; Xiong, K.; Bian, K.; Zhu, K. Experimental Study and Electromechanical Model Analysis of The Nonlinear Deformation Behavior of IPMC Actuators. *Acta Mech. Sin.* **2017**, *33*, 382–393.

(48) Wang, H. S.; Cho, J.; Song, D. S.; Jang, J. H.; Jho, J. Y.; Park, J. H. High-Performance Electroactive Polymer Actuators Based on Ultrathin Ionic Polymer–Metal Composites With Nanodispersed Metal Electrodes. *ACS Appl. Mater.* **2017**, *9*, 21998–22005.

(49) Aureli, M.; Lin, W.; Porfiri, M. On the Capacitance-Boost of Ionic Polymer Metal Composites Due to Electroless Plating: Theory and Experiments. *J. Appl. Phys.* **2009**, *105*, 104911.

(50) Yu, Q.; Guo, F. M.; Wang, X. D.; Stähl, K.; Ren, Y.; Cao, Q. P.; Zhang, D. X.; Jiang, J. Z. Structural Evolution of Low-Temperature Liquid GaIn Eutectic Alloy. *J. Mol. Liq.* **2019**, *293*, No. 111464.

(51) Mirvakili, S. M.; Hunter, I. W. Vertically Aligned Niobium Nanowire Arrays for Fast-Charging Micro-Supercapacitors. *Adv. Mater.* **2017**, *29*, No. 1700671.

(52) Takeuchi, I.; Asaka, K.; Kiyohara, K.; Sugino, T.; Terasawa, N.; Mukai, K.; Shiraishi, S. Electromechanical Behavior of A Fully Plastic Actuator Based on Dispersed Nano-Carbon/Ionic-Liquid-Gel Electrodes. *Carbon* **2009**, *47*, 1373–1380.

(53) Mirvakili, S. M.; Mirvakili, M. N.; Englezos, P.; Madden, J. D. W.; Hunter, I. W. High-Performance Supercapacitors From Niobium Nanowire Yarns. *ACS Appl. Mater. Interfaces* **2015**, *7*, 13882–13888.

(54) Martins, J. C.; Neto, J. C. M.; Passos, R. R.; Pocrifka, L. A. Electrochemical Behavior of Polyaniline: A Study by Electrochemical Impedance Spectroscopy (EIS) in Low-Frequency. *Solid State Ionics* **2020**, *346*, No. 115198.

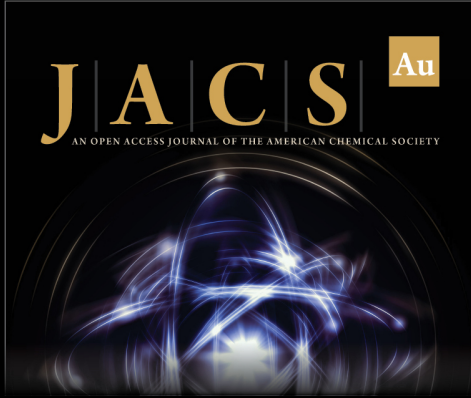
(55) Mei, B. A.; Munteshari, O.; Lau, J.; Dunn, B.; Pilon, L. Physical Interpretations of Nyquist Plots for EDLC Electrodes and Devices. *J. Phys. Chem. C* **2018**, *122*, 194–206.

(56) He, Q.; Yu, M.; Yang, X.; Kim, K. J.; Dai, Z. An Ionic Electro-Active Actuator Made with Graphene Film Electrode, Chitosan and Ionic Liquid. *Smart Mater. Struct.* **2015**, *24*, No. 065026.

(57) Olsen, Z. J.; Kim, K. J. A Hyperelastic Porous Media Framework for Ionic Polymer-metal Composite Actuators and Sensors: Thermodynamically Consistent Formulation and Non-dimensionalization of The Field Equations. *Smart Mater. Struct.* **2021**, *30*, No. 095024.


(58) Biswal, D. K.; Bandyopadhyay, D.; Dwivedy, S. K. A Non-linear Dynamic Model of Ionic Polymer-metal Composite (IPMC) Cantilever Actuator. *Int. J. Automot. Technol.* **2019**, *16*, 6332–6347.


(59) Fedrigo, W.; Núñez, W. P.; López, M. A. C.; Kleinert, T. R.; Ceratti, J. A. P. A Study on The Resilient Modulus of Cement-treated Mixtures of RAP and Aggregates Using Indirect Tensile, Triaxial and Flexural Tests. *Constr. Build. Mater.* **2018**, *171*, 161–169.



JACS Au
AN OPEN ACCESS JOURNAL OF THE AMERICAN CHEMICAL SOCIETY

Editor-in-Chief
Prof. Christopher W. Jones
Georgia Institute of Technology, USA

Open for Submissions 

pubs.acs.org/jacsau  ACS Publications
Most Trusted. Most Cited. Most Read.